ELSEVIER

Journal of Alloys and Compounds 433 (2007) 356–362

Journal of ALLOYS AND COMPOUNDS

www.elsevier.com/locate/jallcom

Crystallization of $Nd_2Fe_{17}B_x$ from stoichiometric melt composition

J. Gao [a,b,*], T. Volkmann [a], S. Yang [d], S. Reutzel [a,c], D.M. Herlach [a], X.P. Song [d]

[a] *Institute of Space Simulation, German Aerospace Center (DLR), 51170 Cologne, Germany*
[b] *Key Laboratory of Electromagnetic Processing of Materials, Northeastern University, Shenyang 110004, China*
[c] *Institute of Experimental Physics IV, Ruhr-University, 44780 Bochum, Germany*
[d] *Department of Materials Physics, Xi'an Jiaotong University, Xi'an 710049, China*

Received 19 June 2006; received in revised form 25 June 2006; accepted 26 June 2006
Available online 31 July 2006

Abstract

Containerless solidification of gas-atomized $Nd_{10}Fe_{85}B_5$ melt droplets was carried out using the drop tube technique. The phase constituents and microstructure of the solidified samples were investigated by means of powder X-ray diffraction analysis, thermomagnetic analysis, and scanning electron microscopy. Besides α-Fe and $Nd_2Fe_{14}B$, non-equilibrium phases such as $Nd_2Fe_{17}B_x$, ε-Nd, and $Nd_{1.1}Fe_4B_4$ were identified. The microstructure of the samples was categorized into three types, including a quasi-single phase one that consists mainly of $Nd_2Fe_{17}B_x$ dendrites. The lattice parameters and Curie temperature of $Nd_2Fe_{17}B_x$ were determined, and compared with those of the same type phase crystallized in Nd-rich Nd–Fe–B melt compositions. The results were discussed with respect to the stoichiometry, formation as well as potential application of $Nd_2Fe_{17}B_x$.

Keywords: Rare earth alloys; Rapid-solidification; Microstructure; SEM; X-ray diffraction

1. Introduction

Solidification of commercial Nd–Fe–B alloys involves primary crystallization of Fe-rich solid solution (γ-phase) as well as subsequent peritectic formation of the $Nd_2Fe_{14}B$ compound (ϕ-phase) from the liquid phase [1]. Previous work [2,3] has shown that liquid undercooling, achieved by electromagnetic levitation or by drop tube processing, can alter the solidification pathway of Nd–Fe–B alloys drastically. On the one hand, liquid undercooling can suppress primary γ-Fe crystallization in favor of direct crystallization of $Nd_2Fe_{14}B$. On the other hand, liquid undercooling can induce crystallization of a metastable intermetallic compound, χ-$Nd_2Fe_{17}B_x$ ($x \sim 1$), either as a primary phase or as an intermediate peritectic phase following primary γ-Fe formation. The grains of $Nd_2Fe_{17}B_x$ are decomposed into a fine mixture of γ-Fe plus $Nd_2Fe_{14}B$ in electromagnetically levitated bulk samples, but are preserved at least partially in drop tube-solidified small samples. The measurements on the drop tube-solidified samples have shown that $Nd_2Fe_{17}B_x$ orders ferromagnetically below 373 K with a $TbCu_7$-type hexagonal structure. In terms of recent in situ synchrotron radiation diffraction analyses on electromagnetically levitated bulk samples [4], the structure of $Nd_2Fe_{17}B_x$ has been refined to a Th_2Zn_{17}-type rhombohedral one. The difference between the two structural types lies in the degree of order of rare earth atom and iron atom-pairs [5]. The former has a lower order than that of the latter, and is usually regarded as a disordered variant of the latter. In both structures, boron atoms have been assumed to occupy interstitial sites. Ozawa et al. [6,7] have also reported crystallization of a metastable intermetallic phase of a Nd_2Fe_{17}-type structure from undercooled Nd–Fe–B melts, which is assumed to be identical to $Nd_2Fe_{17}B_x$. In the present work, gas-atomized $Nd_{10}Fe_{85}B_5$ melt droplets were containerlessly undercooled and solidified using the drop tube technique in order to check if $Nd_2Fe_{17}B_x$ can be crystallized from stoichiometric melt composition.

2. Experimental

Alloys with atomic composition of $Nd_{10}Fe_{85}B_5$ were prepared by arc-melting elemental Nd (99.9% purity), Fe (99.995 purity) and B (99.995% purity) under the protection of an argon atmosphere (99.999% purity). In order to compensate for mass loss during arc-melting and subsequent induction melting, an

* Corresponding author. Present address: Northeastern University, Key Laboratory of Electromagnetic Processing of Materials, Shenyang 110004, China. Tel.: +86 24 8368 1915; fax: +86 24 8368 1758.
E-mail address: jgao@mail.neu.edu.cn (J. Gao).

0925-8388/$ – see front matter © 2006 Elsevier B.V. All rights reserved.
doi:10.1016/j.jallcom.2006.06.090

extra mass of about 1% was added both for Nd and for B. An alloy was placed in a quartz tube with a small nozzle of 0.5 mm in diameter at the bottom. The quartz tube was inserted into an induction melting coil fixed at the top part of an 8-m drop tube. After evacuation to a pressure of 10^{-4} Pa, the drop tube was back-filled with helium gas (99.999% purity) to a pressure of 5×10^4 Pa. The alloy was melted and overheated using the induction melting technique. By introduction of an overpressure into the quartz tube, the melt was ejected out of the nozzle, and atomized into fine droplets of diameter ranging from 0.3 to 1.6 mm. Most of the droplets were solidified during free fall, and hence showed a round geometry after solidification. Two drop tube experiments were conducted under identical conditions (alloy mass, gas pressure, overheating temperature, etc.). The samples of one experiment was used for powder X-ray diffraction analysis (XRD) and for thermomagnetic analysis (TMA), whereas those of another experiment for microstructural investigations. In the XRD analysis, Fe Kα radiation ($\lambda = 0.1937$ nm) was chosen in order to avoid overlapping of the diffraction peaks from α-Fe and $Nd_2Fe_{14}B$. The TMA was performed with a Lake Shore vibrating sample magnetometer (VSM). The samples were heated and cooled in a crude vacuum, while a magnetic field of 400 kA/m was applied. The Curie temperature of ferromagnetic phase constituents was determined by intersecting linear extensions of a TMA curve around a ferromagnetic transition. The samples for microstructural investigations were sieved into several size groups, and mounted in an epoxy resin. After grinding and polishing, the samples were examined with a LEO1530VP scanning electron microscope (SEM) under back-scattering imaging conditions. The Nd and Fe concentrations of phase constituents were analyzed using an energy dispersive X-ray microanalyzer (EDX) attached to the SEM.

3. Results

The pseudo-binary Fe-$Nd_2Fe_{14}B$ phase diagram of the ternary Nd–Fe–B system [1] is represented in Fig. 1. The alloy composition under study lies in the primary crystallization field of γ-Fe, and its room temperature phase constituents should be α-Fe plus $Nd_2Fe_{14}B$. However, the powder XRD analysis demonstrated that besides the two phases, three non-equilibrium phases exist in the present samples. As shown in Fig. 2, large-sized samples contain the hexagonal ε-Nd phase (usually known as Nd-rich phase) and the tetragonal $Nd_{1.1}Fe_4B_4$ compound (η-phase), whereas small-sized samples contain the metastable $Nd_2Fe_{17}B_x$. Special attention was paid to $Nd_2Fe_{17}B_x$. Indexing of its diffraction peaks to a rhombohedral lattice yielded lattice

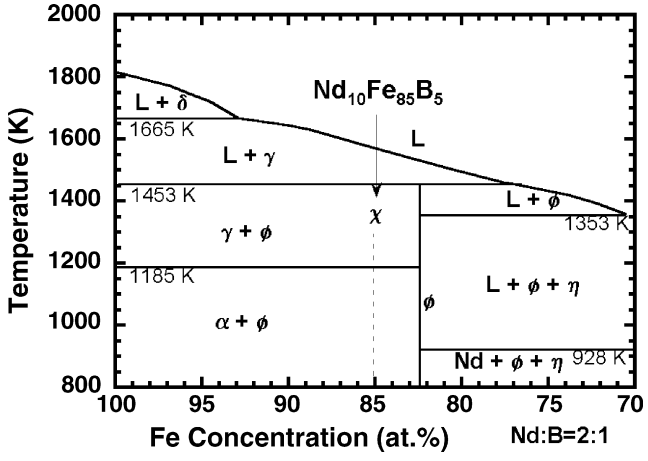

Fig. 1. Pseudo-binary Fe-$Nd_2Fe_{14}B$ phase diagram of the ternary Nd–Fe–B system reproduced from Ref. [1]. The vertical dashed line shows the stoichiometry of a metastable phase crystallized from the undercooled liquid, which coincides the alloy composition under study.

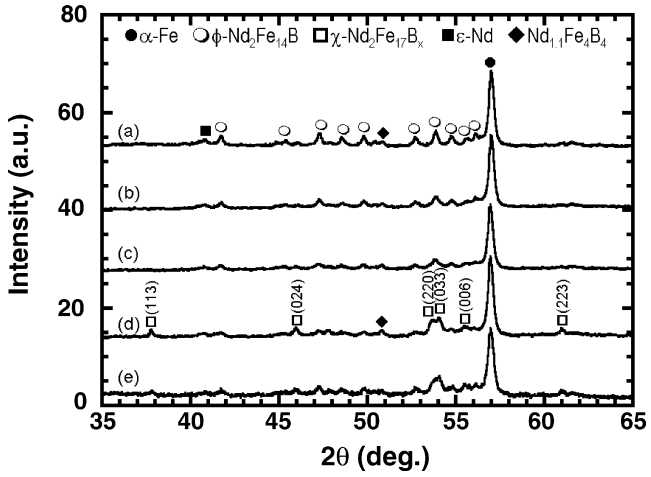

Fig. 2. Powder X-ray diffractions of the solidified samples of different sizes. (a) 1.2–1.6 mm; (b) 1.0–1.2 mm; (c) 0.8–1.0 mm; (d) 0.6–0.8 mm; (e) 0.3–0.6 mm.

parameters as $a = 0.856$ nm and $c = 1.265$ nm. For comparison, the same diffraction peaks obtained in previous work [3,8] were re-indexed to the rhombohedral lattice, and the results are listed in Table 1. It is noted that a keeps constant, and is comparable to that of the binary Nd_2Fe_{17} compound. On the other hand, c decreases slightly with increasing Nd concentration of the melt composition, and becomes very close to that of the binary Nd_2Fe_{17} at a Nd content of 16 at.%. Like the XRD patterns, the TMA curves also show a sample size-dependence. As illustrated in Fig. 3a, large-sized samples undergo a ferromagnetic transition around a Curie temperature of $T_{c1} \sim 600$ K, indicating the presence of $Nd_2Fe_{14}B$ with a well-recognized Curie temperature of 585 K. Additionally, large-sized samples show a non-zero magnetic moment at the high temperature end of the curve, implying that there exists another ferromagnetic phase of a Curie temperature higher than 773 K. By reference to the above XRD analysis (Fig. 2), the second ferromagnetic phase was assumed to be α-Fe ($T_c \sim 1143$ K). For medium-sized samples,

Table 1
Lattice parameters and Curie temperature of $Nd_2Fe_{17}B_x$ grains crystallized in different alloy compositions

Alloy composition (at.%)	Lattice parameters		Curie temperature T_c (K)	Reference
	a (nm)	c (nm)		
$Nd_{16}Fe_{76}B_8$	0.8567	1.247	–	[8]
$Nd_{14}Fe_{79}B_7$	0.8578	1.256	327–338	[6]
$Nd_{11.8}Fe_{82.3}B_{5.9}$	0.8561	1.264	365	[2]
	0.8548	1.264	–	[7]
$Nd_{10}Fe_{85}B_5$	0.8558	1.265	363	Present work
	0.8552	1.268	353	Present work
Nd_2Fe_{17}	0.8579	1.246	330	[9,10]

The diffraction peaks of $Nd_2Fe_{17}B_x$ in previous work [3,8] were re-indexed to a rhombohedral lattice, and those reported by Ozawa et al. [6,7] were also analyzed. For Nd concentrations of 10, 11.8, and 14 at.%, (1 1 3), (0 2 4), (0 3 3), and (2 2 3) diffractions were used for calculation of the lattice parameters by applying the least square algorithm. For a Nd concentration of 16 at.%, (2 2 0) and (0 3 3) diffractions were used, because they are the only distinguishable diffractions in the XRD patterns.